

HiSST: 4th International Conference on High-Speed Vehicle Science Technology



22–26 September 2025, Tours, France

Coupled Fluid-Structure Simulations of a Clamped Panel at High Speed

Bodo Reimann¹, Marius Franze¹, Sebastian Jack¹, Fynn Barz¹, Viola Wartemann¹

Abstract

To simulate the fluid-structure interaction (FSI) of a clamped panel at high speed the DLR flow solver TAU code is coupled with the commercial structure mechanic solver ANSYS. The investigated case is a thin steel panel mounted flush with the wall of a Mach 2 wind tunnel. The panel is excited by a separated shock-boundary layer interaction in turbulent flow. The simulations are based on experimental test carried out in the RC-19 facility at the Air Force Research Laboratory (AFRL) in Dayton/Ohio. Thermal expansion of the structure caused by aerothermal heating leads to buckling of the panel and a change of the pressure in the closed cavity on the back of the panel. In addition to the effects of thermal heating and cavity pressure change the study investigates the influence of structural damping and of the simulated physical time-step size.

Keywords: CFD/CSM coupling, CoNF²aS², Fluid-structure interaction, FSI, Panel flutter, AePW-4

Nomenclature

Abbreviations		T	Temperature
AePW	Aeroelastic Prediction Workshop	t	Time
AFRL	Air Force Research Laboratory	v_z	Displacement velocity
CFD	Computational fluid dynamics	x, y, z	Cartesian coordinates
CoNF ² aS ²	Coupled Numerical Fluid Flight Mechanics		
	and Structure Simulations	Greek	
CSM	Computational structure mechanics	α	Thermal expansion coefficient
DLR	German Aerospace Center	α_d	Mass damping coefficient
FSI	Fluid-structure interaction	β_d	Stiffness damping coefficient
LCO	Limit cycle oscillation	ν	Poisson ratio
PSD	Power spectral density	ho	Density
Latin			
a	Panel length	Subscripts	
b	Panel width	∞	Free stream values
c	Cavity height	0	Total values
E	Young modulus	c	Cavity values
d	Panel thickness	f	Frame values
M	Mach number	init	Initial values
p	Pressure	p	Panel values

1. Introduction

Aerothermodynamic loads on high speed vehicles and the structural response of its surface lead to a coupled physical problem. The behavior of this fluid-structure interaction (FSI) is often non-linear and path-dependent. The effects on the structure ranges from capacitive cooling to melting of the structure and from steady thermal buckling to limit cycle oscillations (LCO) or chaotic flutter behavior up to mechanical structural failure. For modern high-speed vehicles optimised in terms of flight performance

HiSST 2025-0258

¹German Aerospace Center (DLR). Institute of Aerodynamics and Flow Technology, Spacecraft, Lilienthalplatz 7, 38108 Braunschweig, Germany, Corresponding author: bodo.reimann@dlr.de

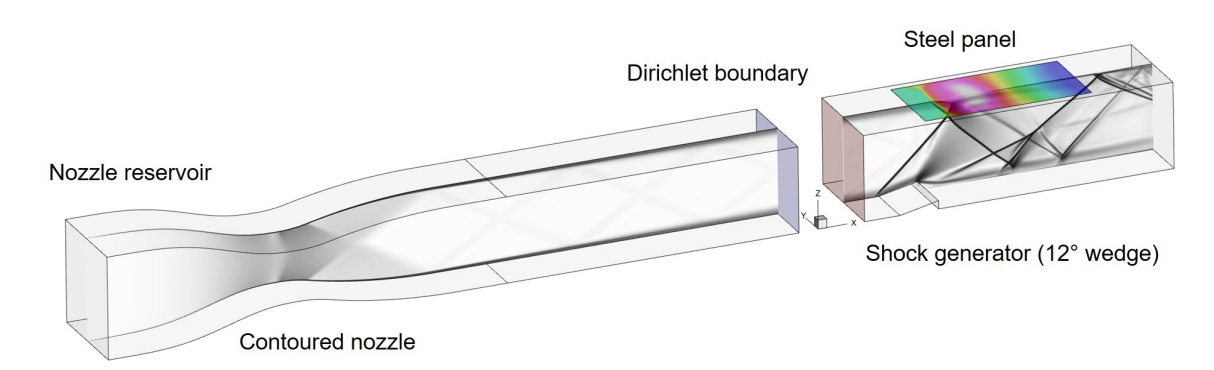


Fig 1. Computational domain of the AFRL RC-19 wind tunnel with flexible steel panel and shock generator.



Fig 2. RC-19 test section flow. On the left a simulated shadowgraph in the center plane of the test section is shown. The right side shows the panel surface pressure distribution.

and mass, these effects play an increasingly important role. The reliable prediction of such behaviour requires consideration of the coupling between the flow field and the vehicle structure and still represents a major challenge for numerical modelling. This paper presents DLR simulation results achieved by coupling the DLR CFD code TAU with the commercial structure mechanic solver ANSYS. To study the physical mechanisms that drive aerothermoelastic FSI instabilities, the accuracy of different levels of fidelity and the influence of model parameters a generic rectangular flexible metallic panel in supersonic flow with shock wave impingement has been selected as test case.

2. Test Case Description and Set-up

The test case consists of a flexible steel panel mounted flush with the wall of a Mach 2 rectangular wind tunnel test section. The simulations are based on tests carried out in the RC-19 facility at the US Air Force Research Laboratory (ARFL) in Dayton/Ohio [2, 3, 4]. Some of the test results were made available as validation tests for the High Speed Working Group (HSWG) as part of the Aeroelastic Prediction Workshop 3 and 4 (AePW-3&4). The numerical set-up and a steady-state flow solution are shown in fig. 1. The exit of a contoured Mach 2 nozzle merges into a rectangular channel. The cross section of the channel is $131.1 \times 152.4 \, \text{mm}$. The size of the panel is $253.9 \times 127.0 \times 0.635 \, \text{mm}$. In the case with shock impingement a wedge on the opposite side of the test section acts as shock generator. The center plane of the channel in fig. 1 shows a simulated shadowgraph of the flow for an undeformed panel. The panel shows the surface pressure distribution. Both results of a stationary calculation, the starting point for the fully coupled FSI simulation. To avoid the expansive simulation of the complete flow domain during the unsteady FSI coupling simulation a Dirichlet boundary condition has been applied. The upstream part of the facility, containing the nozzle and the upstream part of the channel, is computed separately. The flow profile at the outflow plane (blue surface) is used as inflow condition (red surface) for the test section. Figure 2 shows an enlarged view of the test section flow. The simulated shadowgraph shows the shock wave structure in the centerplane of the test section. The oblique shock wave in front of the wedge interacts with the viscous boundary layer on the flexible

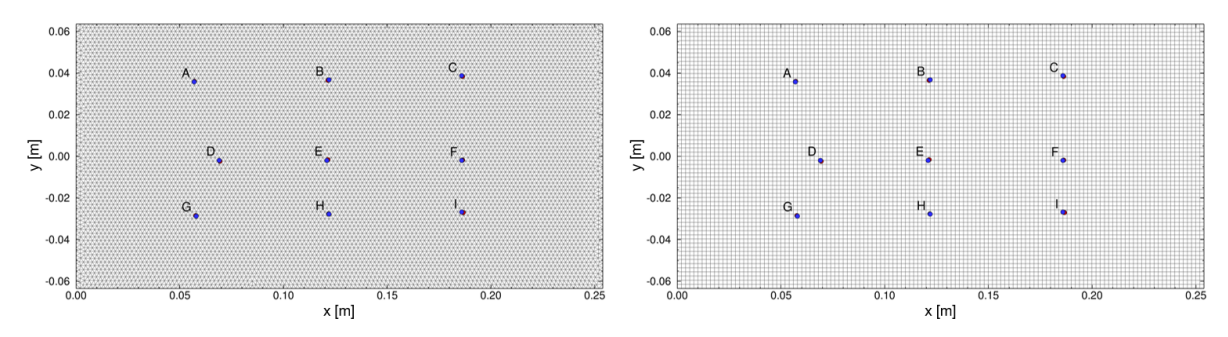


Fig 3. Panel mesh for CFD (left) and CSM solver (right). The points A to I represent sensor positions. The cell size is around 2 mm.

$\overline{p_0}$	[kPa]	344.85		
T_0	[K]	385.82		
$p_{c,init}$	[kPa]	92.355		
$a\times b\times d$	[mm]	$253.9 \times 127.0 \times 0.635$		
ρ	[kg m ⁻³]	7850		
ν	[-]	0.27		
E	[GPa]	208.0		
α	[K ⁻¹]	$12.2\cdot 10^{-6}$		
α_d	[s ⁻¹]	15		
β_d	[s]	$8 \cdot 10^{-7}$		
T_p	[K]	367.97		
T_{f}	[K]	355.97		

Table 1. Test condition and panel data.

panel. A further oblique shock wave occurs in front of the separation bubble that interacts with the primary shock wave forming a Mach reflection pattern. On the right the surface pressure distribution on the panel is plotted. The pressure jump marks the position of the separation shock. Due to the interaction with the boundary layer along the side walls of the channel the pressure isolines are slightly curved.

Figure 3 shows the discretization of the panel mesh for the fluid and structure domain. The fluid mesh consists of triangles while the structure mesh consists of quadrilaterals. The CFD volume mesh of triangular prism and tetrahedrons has 23.3 million points and a maximum cell size of 2 mm.

The gas is assumed to be calorically perfect air. All walls are modeled as adiabatic non-slip fully turbulent boundaries. A Reynolds Stress Model (RSM) turbulence model is used. All relevant simulation parameters for the flow and the pane are listed in tab. 1. The pressure on the back of the panel is the cavity pressure p_c . The Mach number of the free stream in the inflow plane of the test section is around 1.92. The panel and its outer frame consists of a single part of ASIS 4140 alloy and is manufactured by milling out a solid block. The advantage of this method, in contrast to gluing, welding or other fastening methods, is a clearly defined mechanical and thermal interface condition between panel and frame.

During the wind tunnel run the walls and especially the panel is heated by the flow. Thin structures heat up much faster than thicker ones, so that the frame acts as a heat sink for the panel. This effect leads to a temperature difference ΔT between panel and frame and thus to thermal stresses due to thermal expansion. These thermal stresses, together with the pressure difference between the test section and the cavity, cause the panel to buckle. In the simulations the temperature difference effect is modelled

HiSST 2025-0258

in the structure mechanic solver. The temperature of the panel T_p is set to constant homogeneous value, while the temperature of the frame T_f (reference temperature) is lowered by the difference of $\Delta T=12\,\mathrm{K}$. Due to the deformation of the panel the volume of the closed cavity V_c above the panel is not longer constant. The cavity pressure p_c is calculated as a function of the volume according to

$$p_c(t) = \frac{p_{c,\text{init}} \, V_{c,\text{init}}}{V_{c,\text{init}} - \Delta V_c(t)} \qquad \text{with} \qquad \Delta V_c(t) = \iint\limits_{\text{panel}} \Delta z(x,y,t) \, \mathrm{d}x \, \mathrm{d}y \tag{1}$$

and the values of volume and pressure for the rigid undeformed panel $V_{c,\text{init}}$ and $p_{c,\text{init}}$, respectively. Figure 4 shows a schematic representation of the cavity and the panel.

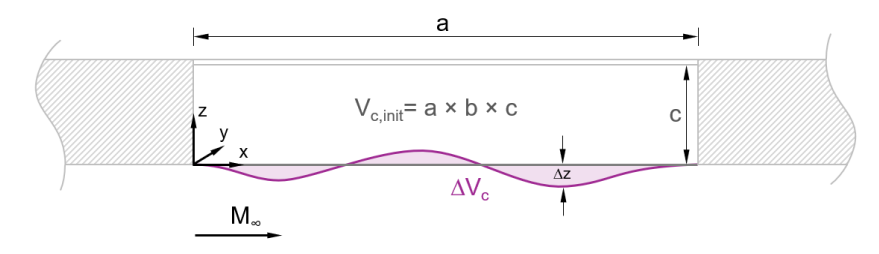


Fig 4. Schematic view of the variable cavity volume caused by the panel deformation.

3. Numerical Method

The DLR CFD solver TAU-Code [10, 7] uses the finite volume method to discretize Euler or Navier-Stokes equations on unstructured grids. Based on the primary grid an edge-based metric called dual-grid is generated in a pre-processing step. If multi-grid technique is used, the pre-processor also agglomerates coarser levels of the dual-grid. Domain splitting is done by the pre-processor as well in case of parallel computations. In the solver module inviscid terms are computed employing either a second-order central scheme or an AUSMDV upwind scheme using linear reconstruction to get second-order spatial accuracy. Viscous terms are generally computed with a second-order central scheme. For time integration various explicit Runge-Kutta schemes, as well as an implicit approximate factorization lower-upper symmetric Gauss-Seidel scheme (LU-SGS) is implemented. For time accurate computations a Jameson-type dual time stepping approach is employed. Additional convergence acceleration is achieved by explicit residual smoothing. To simulate turbulent flows the user has the choice between several one- and two-equation turbulence models, a Reynolds stress or a DES model. The code has the capability to simulate perfect gas

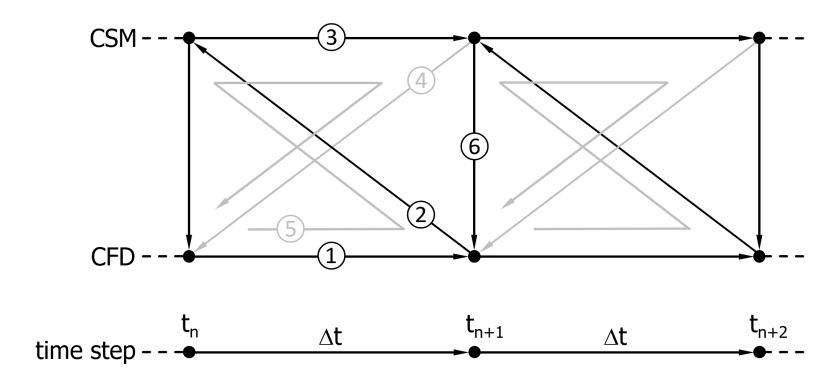


Fig 5. CFD/CSM coupling scheme. ① computation of CFD time-step, ② exchange of aerodynamic loads, ③ computation of CSM time-step, ④ exchange of structural deformation and mesh deformation ⑤ repetition of step ① to ④ until convergence. ⑥ exchange of converged deformation state.

flows as well as flow in thermo-chemical non-equilibrium. The TAU code provides local grid refinement and grid deformation. For the unsteady simulation of the buckling and vibrating panel the robustness of the mesh deformation is important. The implicit volume mesh deformation method based on linear elasticity analogy and is described in detail in [9].

The commercial structure mechanical analysis software Ansys Mechanical [1] was used to simulate the deformation of the structure. Within the solver the finite element method was applied to solve the discrete equations of motion for each local cell. Structural damping is modelled using the Rayleigh approach with damping coefficient for mass and stiffness.

To simulate FSI the DLR flow solver TAU-Code is coupled with the structure mechanical solver Ansys Mechanical within the FlowSimulator [6] software environment. The coupled CFD/CSM problem is solved in a partitioned manner. A so-called strong coupling scheme [5, 8] is used. Strong coupling means that the coupled equations are iteratively solved within each physical time-step by repeatedly solving the involved disciplines CFD and CSM separately based on the exchanged coupling quantities. These are on CFD side aerodynamic loads (forces and moments) and on CSM site the deformation state of the structure (displacement and velocities). The coupling scheme performs one predictor and a number of corrector steps. The corrector steps are terminated until the deformation update falls below a predefined threshold. If the corrector steps are set to zero, the strong coupling scheme turns into a week coupling scheme. The operation chart of the partitioned strong coupling approach between CFD and CSM is shown in fig. 5.

Starting from a converged solution at time-step n the CFD solver computes the aerodynamic loads at the next time-step n+1 (1), these loads are interpolated onto the structural domain (2). Based on the loads the CSM solver computes the actual deformation for the time-step n+1 (3). The deformations are interpolated to the fluid domain, the mesh is deformed and the change of the cavity pressure is computed (4). This loop is than repeated for the same time-step until the difference of the norm of the displacement vector of two consecutive inner loops (coupling residual) is less than a given limit (5). After cancelling the loop, the converged deformation state is passed to the flow solver for the calculation of the next time-step n+2.

4. Results

During the wind tunnel run the walls and especially the panel is heated by the flow. The thin panel heats up much faster than the thicker frame. This effect leads to a temperature difference between panel and frame. The results show a significant effect on the oscillation behavior on the temperature difference. Figure 6 shows on the left the oscillation of the center point of the panel (point E, see fig. 3) in the phase-space. Shown are only data after the transient phase. The closed trajectories are an indicator for a LCO. The trajectory shows a larger oscillation amplitude and a larger velocity of the considered point if the temperature difference increases. The reason is the structural buckling due to the thermal expansion. On the right of fig. 6 the corresponding power spectral density (PSD) is shown. The PSD shows how the power of a signal or a time series is distributed with frequency. The PSD of the center point oscillation is compared with experimental results provided by AFRL. The buckling effect leads to a significant shift of the first dominant oscillation mode towards a lower frequency, an thus closer to the measured values.

The phase-space plot in fig.6 show trajectories computed with different time-steps for the case with $\Delta T=12\,\mathrm{K}.$ The large difference of the results is the reason to examine the influence of the time-step more closely. Figure 7 shows simulation results computed with five different time-steps. Convergence with respect to the time-step is not achieved. The smaller the simulated physical time-step, the higher the resolved frequency components. The high spatial resolution of the panel also allows the occurrence of modes with large wave numbers. For $\Delta t < 0.025\,\mathrm{ms}$ the PSD in fig. 6 shows the same characteristic peaks especially for the first four oscillation modes. From a theoretical point of view, with this time-step oscillations with frequencies up to $20000\,\mathrm{Hz}$ can be resolved. An issue with the evaluation of the PSD is, that the evaluation interval shrinks as the time-step decreases due to the higher simulation effort.

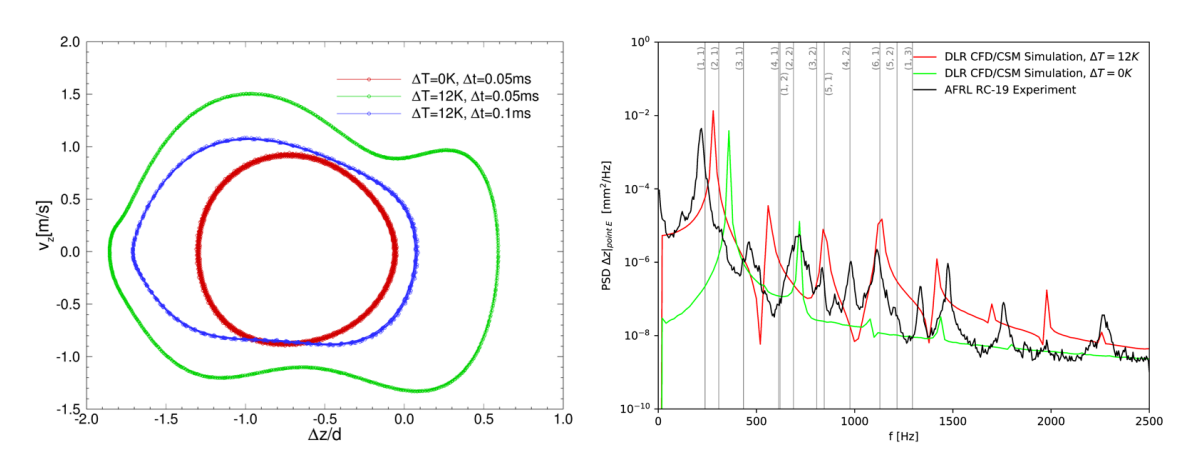


Fig 6. Phase-space trajectory (left) and PSD (right) of the panel center. The simulations have been carried out for different temperature differences ΔT between panel and frame. The PSD plot also shows the natural modes and frequencies of the panel.

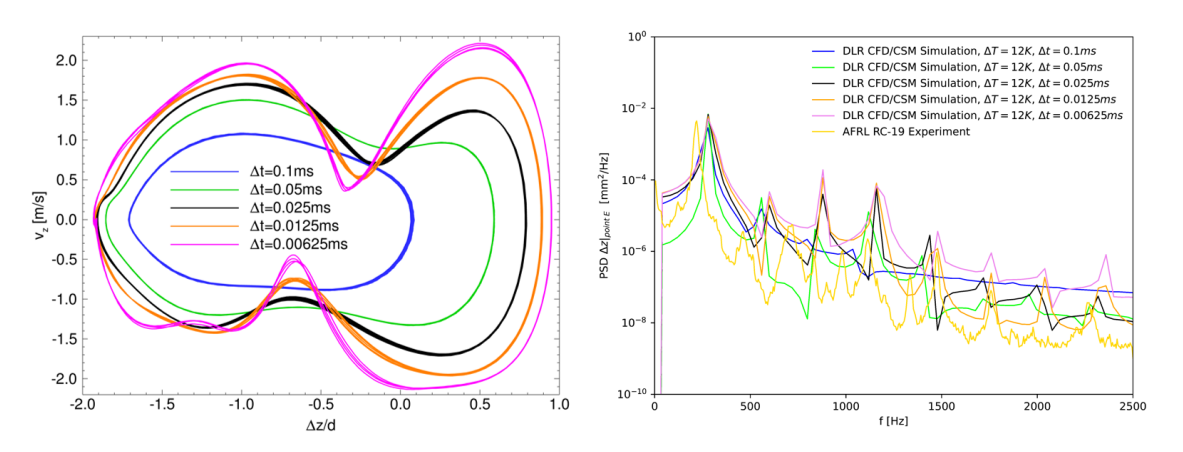


Fig 7. Phase-space trajectory (left) and PSD (right) of the panel center. The simulations have been carried out with different physical time-steps Δt .

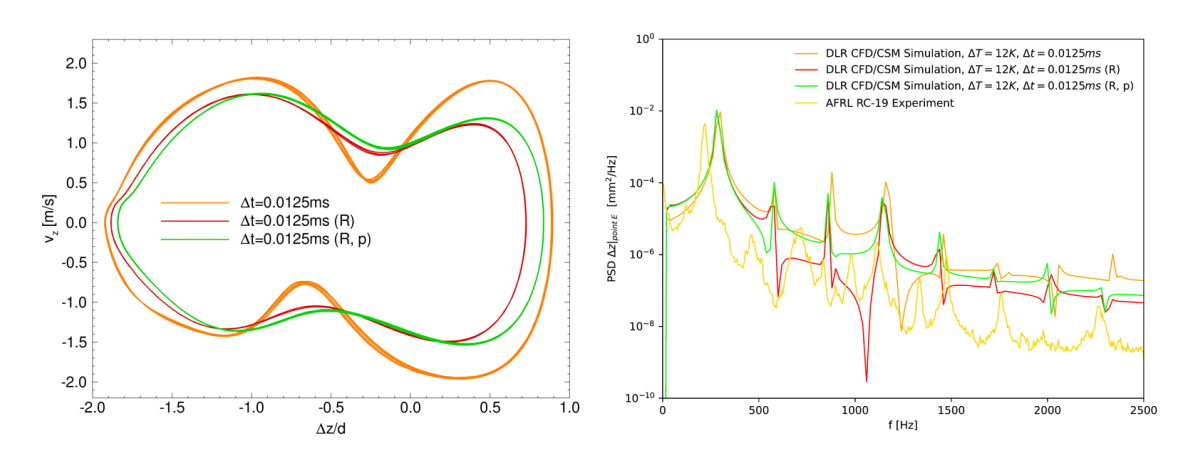


Fig 8. Phase-space trajectory (left) and PSD (right) of the panel center. All simulations have been carried out for a time-step of $\Delta t=0.0125\,\mathrm{ms}$ and take into account structural damping (R) and structural damping plus variable cavity pressure (R, p).

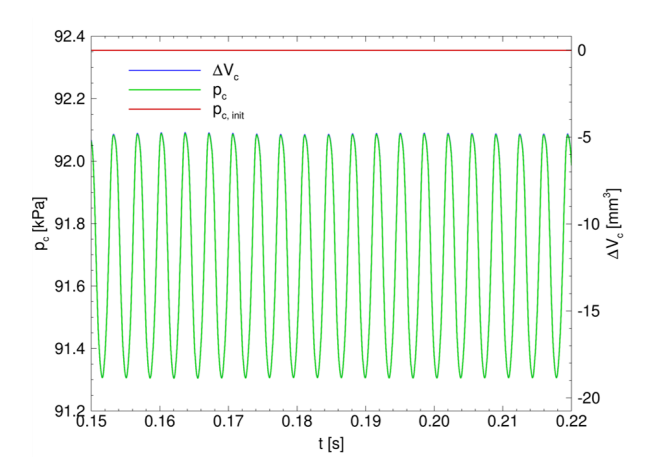


Fig 9. Cavity pressure p_c and cavity volume change ΔV_c over time t. Cavity pressure and volume change are congruent. If the volume change is neglected, the cavity pressure is equal to the initial cavity pressure $p_{c, \mathsf{init}}$.

The results shown so far neglect the structural damping and the change of the cavity pressure. For the structural damping the Rayleigh formulation is applied within the CSM solver using the coefficients for mass and stiffness given in tab. 1. The cavity pressure is computed and set within each correction loop based on the deformation of the panel according to eq. 1. Based on the previous results a time-step of $\Delta t = 0.0125$ ms has been selected for these simulations. Figure 8 show the influence of structural damping and structural damping plus cavity pressure change on the center point oscillation. Structural damping decreases the panel displacement as well as the displacement velocity. The effect of the timedependent cavity pressure is small. In the present case, the pressure changes periodically by ± 0.4 kPa around the mean value as shown in fig. 9. The inertial cavity pressure was assumed for a flat, nondeformed panel. This is not quite correct. Rather, the inertial pressure should be assumed for a panel that has already been thermally buckled. The buckling increases the volume and decreases the cavity pressure. This is the reason why the mean value of the cavity pressure is below the initial cavity pressure. Ideally, mean pressure and inertial pressure should be the same. A time-history plot of the normalized panel displacement along the mid-span of the panel is plotted in fig. 10. The results show very good a with experimental AFRL results published by Brouwer et al. [2].

5. Summary and Outlook

Fully coupled CFD/CSM simulations of a thin steel panel excited by a separated shock-boundary layer interaction in fully turbulent flow have been performed. The numerical simulations take into account thermal expansion, structural damping, and the dynamically changing cavity pressure. The influence of the simulated time-step Δt is investigated in a time-step convergence study. After a transient phase all results show a LCO. The comparison with the experimental test data received by AFRL is very good. The results show that the aerothermal heating of the material is the dominant effect. The thermal expansion of the clamped panel has a significant influence on the flutter characteristics like amplitude and frequencies. The other main effect not investigated here in detail is the mean cavity pressure [2]. The simulation of small physical time-steps leads to the resolution of high-frequency components. On the other side the large number of degrees of freedom in the structural mesh allows mode shapes with large wave numbers. Many studies in this field use reduced order models (ROM) with a fixed number of mode shapes and a limited frequency domain to compute the structural response. For the present simulation strategy the choice of the time-step should be made depending on the frequency range of interest. The mode shapes that occur have not yet been analysed in the present study, this is planned as part of further investigations. The coupled CFD/CSM simulation are extremely time consuming and not suitable for calculating an entire parameter space such as panel temperature or cavity pressure. A

HiSST 2025-0258

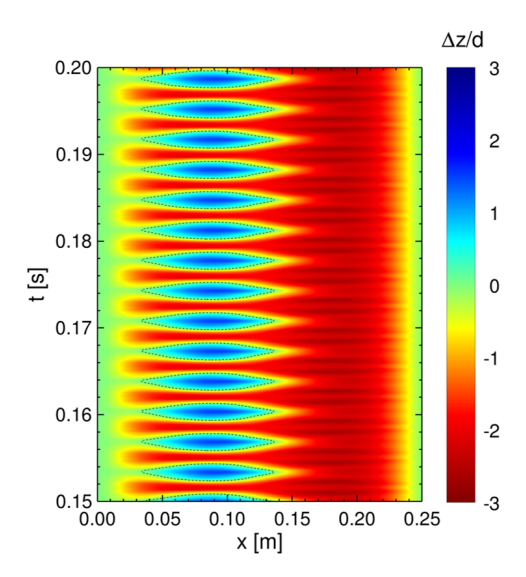


Fig 10. LCO along panel mid-span. Normalized panel displacement $\Delta z/d$ along the mid-span y/b=0.5 of the panel versus time t. Plotted are the simulation results for a time-step of $\Delta t=0.0125\,\mathrm{ms}$ including variable cavity pressure and structural damping. The plot uses a similar representation as chosen for the experimental AFRL results shown by Brouwer *et al.* [2].

large number of studies use low fidelity methods like ROMs on the structural side and classical piston theory on the fluid mechanic side. The methods are fast and much more suitable to simulate an entire parameter space to find relevant one. But often these methods fail to predict more complex cases like the one shown here with separated shock boundary layer interaction. The intention to develop and apply the strongly coupled approach of a finite-volume based flow solver with a finite-element based structure solver as described here, is to be able to simulate arbitrary geometries and materials in the future.

Acknowledgements

The simulation results shown are part of a study founded by the German Federal Ministry of Defense under contract no. E/K2AL/NA060/HF132 (HYRECA). The authors would like to thank the Air Force Research Laboratory for providing experimental data. Thanks also to the AFRL team and the High Speed Working Group as part of the Aeroelastic Prediction Workshop for fruitful discussions and sharing of experience. The authors also gratefully acknowledges the TAU code development team at the German Aerospace Center (DLR),as well as the scientific support and HPC resources provided by DLR. The HPC system CARA is partially funded by the Saxon State Ministry of Economic Affairs, Labour and Transport and the Federal Ministry of Economics and Climate Protection.

References

- [1] ANSYS, Inc. Ansys Mechanical Finite Element Analysis Software for Structural Engineering, 2025. URL https://www.ansys.com/products/structures/ansys-mechanical.
- [2] K. R. Brouwer, R. A. Perez, T. J. Beberniss, S. M. Spottswood, and D. A. Ehrhardt. Experiments on Thin Panel Excited by Turbulent Flow and Shock/Boundary-Layer Interaction. *AIAA Journal*, 59 (7):2737–2751, 2021. https://doi.org/10.2514/1.J060114.
- [3] K. R. Brouwer, R. A. Perez, T. J. Beberniss, S. M. Spottswood, D. A. Ehrhardt, and R. Wiebe. Investigation of aeroelastic instabilities for a thin panel in turbulent flow. *Nonlinear Dynamics*, 14 (7):3323–3346, 2021. https://doi.org/10.1007/s11071-021-06571-4.
- [4] K. R. Brouwer, R. A. Perez, T. J. Beberniss, S. M. Spottswood, and D. Ehrhardt. Evaluation of

- reduced-order aeroelastic simulations for shock-dominated flows. *Journal of Fluids and Structures*, 108, 2022. https://doi.org/10.1016/j.fluidstructs.2021.103429.
- [5] R. Heinrich, L. Reimer, and A. Michler. Multidisciplinary simulation of maneuvering aircraft interacting with atmospheric effects using the DLR TAU code, 2011. RTO AVT-189 Specialists' Meeting on Assessment of Stability and Control Prediction Methods for Air and Sea Vehicles.
- [6] I. Huismann, L. Reimer, S. Strobl, J. Eichstädt, R. Tschüter, A. Rempke, and G. Einarson. Accelerating the FlowSimulator: Profiling and scalability analysis of an industrial-grade CFD-CSM toolchain. In 9th International Conference on Computational Methods for Coupled Problems in Science and Engineering. Virtual event, 2021.
- [7] S. Langer, A. Schwöppe, and N. Kroll. In *AIAA 52nd Aerospace Sciences Meeting*. National Harbor/Maryland, USA, 2014. https://doi.org/10.2514/6.2014-0080.
- [8] L. Reimer, R. Heinrich, and R. Meurer. Validation of a Time-Domain TAU-Flight Dynamics Coupling Based on Store Release Scenarios. *Notes on Numerical Fluid Mechanics an Multidisciplinary Design*, 124:455–463, 2014. https://doi.org/10.1007/978-3-319-03158-3_46.
- [9] A. Rempke. Deformation of CFD Meshes with Anisotropic Cells in a Viscous Boundary Layer Using Line-Implicit Methods. New Results in Numerical and Experimental Fluid Mechanics XIV. STAB/DGLR Symposium 2022. Notes on Numerical Fluid Mechanics an Multidisciplinary Design, 154:273–283, 2024. https://doi.org/10.1007/978-3-031-40482-5_26.
- [10] D. Schwamborn, T. Gerhold, and R. Heinrich. The DLR TAU-Code: Recent Applications in Research and Industry. In *ECCOMAS CFD 2006*. Eggmond aan Zee, The Netherlands, 2006.

HiSST 2025-0258 Page | 9